Lattice Engineering via Transition Metal Ions for Boosting Photoluminescence Quantum Yields of Lead-Free Layered Double Perovskite Nanocrystals

Maning Liu, Sri Kasi Matta, Tarek Al Said, Jiatu Liu, Anastasia Matuhina, Basheer Al-Anesi, Harri Ali-Löytty, Kimmo Lahtonen, Slavy P. Russo, and Paola Vivo*

Lead-free layered double perovskite nanocrystals (NCs), i.e., $Cs_4M(II)M(III)_2Cl_{12}$, have recently attracted increasing attention for potential optoelectronic applications due to their low toxicity, direct bandgap nature, and high structural stability. However, the low photoluminescence quantum yield (PLQY, <1%) or even no observed emissions at room temperature have severely blocked the further development of this type of lead-free halide perovskites. Herein, two new layered perovskites, $Cs_4CoIn_2Cl_{12}$ (CCoI) and $Cs_4ZnIn_2Cl_{12}$ (CZnI), are successfully synthesized at the nanoscale based on previously reported $Cs_4CuIn_2Cl_{12}$ (CCuI) NCs, by tuning the M(II) site with different transition metal ions for lattice tailoring. Benefiting from the formation of more self-trapped excitons (STEs) in the distorted lattices, CCoI and CZnI NCs exhibit significantly strengthened STE emissions toward white light compared to the case of almost non-emissive CCuI NCs, by achieving PLQYs of 4.3% and 11.4% respectively. The theoretical and experimental results hint that CCoI and CZnI NCs possess much lower lattice deformation energies than that of reference CCuI NCs, which are favorable for the recombination of as-formed STEs in a radiative way. This work proposes an effective strategy of lattice engineering to boost the photoluminescent properties of lead-free layered double perovskites for their future warm white light-emitting applications.

1. Introduction

Lead-free halide double perovskite materials[1–4] have become one promising alternative to the conventional lead-based halide perovskites when concerning the high toxicity of the latter case for their practical use.[5–8] Halide double perovskites, with a typical structure $A_2M(I)M(III)X_6$ (e.g., $A = Cs^+$; $M(I) = Ag^+$; $M(III) = Bi^{3+}$, In^{3+}, Sb^{3+}; $X = Cl^-$, B^-), feature low or non-toxicity, high phase stability, and diverse compositional space, which makes them potentially suitable for optoelectronic and photocatalytic applications.[9–12] However, the indirect bandgap nature significantly reduces the optoelectronic functionality of halide double perovskites, leading to a large gap in device performance compared to their lead counterparts. Moreover, the photoluminescence quantum yields (PLQYs) of lead-free halide perovskites are generally low, particularly in the form of nanocrystals,[13,14] due to the high density of intrinsic defects and the insulating

---

M. Liu
Centre for Analysis and Synthesis
Department of Chemistry
Lund University
P.O. Box 124, Lund 22100, Sweden
E-mail: maning.liu@chem.lu.se

M. Liu
Wallenberg Initiative Materials Science for Sustainability
Department of Chemistry
Lund University
Lund 22100, Sweden

The ORCID identification number(s) for the author(s) of this article can be found under https://doi.org/10.1002/smll.202401051

DOI: 10.1002/smll.202401051

M. Liu
NanoLund
Lund University
Lund 22100, Sweden

M. Liu, A. Matuhina, B. Al-Anesi, P. Vivo
Hybrid Solar Cells
Faculty of Engineering and Natural Sciences
Tampere University
P.O. Box 541, Tampere FI-33014, Finland

S. K. Matta
JSPS International Research Fellow (Center for Computational Sciences)
University of Tsukuba
Tsukuba 305-8577, Japan

S. K. Matta
Australian Research Council (ARC) Centre of Excellence for Exciton Science
RMIT University
Melbourne 3000, Australia

effect from long alkyl chain-based capping ligands, which indeed highlights the big challenge in their defect engineering and surface engineering. Very recently, so-called vacancy-ordered layered double perovskites with formula $Cs_4M(II)M(III)_2X_{12}$ (M(II) = Cu^{2+}, Zn^{2+}) have been discovered and synthesized both in the form of single crystals[15,16] and colloidal nanocrystals (NCs),[16–19] demonstrating several intriguing characteristics such as direct bandgap nature, narrow bandgap (down to ≈1.0 eV), low effective masses and superior structural stability. The crystal structure of layered double perovskites consists of one layer of $[M(II)X_6]^{4-}$ octahedra sandwiched by two layers of $[M(III)X_6]^{3-}$ octahedra, which forms an anisotropic conformation.[15] To date, colloidal $Cs_4M(II)Sb_2Cl_{12}$ NCs have been primarily synthesized by tuning the M(II) site with divalent metal ions such as Cu^{2+}[18,19] and Zn^{2+},[16] exhibiting ultrafast photoelectrical response and size-tunable photocatalytic activity, respectively. Nevertheless, the relatively high toxicity of Sb element as well as the lack of observed PL at room temperature (RT) from this kind of $Cs_4M(II)Sb_2Cl_{12}$ NCs restrict their further application. Our recent work[19] has proposed a new system of layered double perovskites by replacing toxic Sb with non-toxic In at M(III) site, resulting in $Cs_4CuIn_2Cl_{12}$ NCs, which shows an almost 2% PLQY at RT in the near UV range upon the moisture-assistance during the synthetic process. We attributed the PL enhancement to the radiative transition of so-called self-trapped excitons (STEs) preferably in the lattices of $[CuCl_6]^{4-}$ octahedra, which were fairly distorted upon the involvement of minor water molecules, i.e., Jahn–Teller distortion.[20,21]

STEs have been widely observed in metal halide crystals, organic molecular crystals as well as condensed rare gases,[22–25] which generally possess soft lattice and strong electron-phonon coupling, leading to an STE emission with a broad spectrum and large Stokes shift. In the context of metal halides, double perovskites have recently emerged as promising STE emitters, due to their 0D electronic dimensionality accompanied by the formation of strong electron-phonon coupling, which is in turn a drawback for solar cells application. Tang et al., significantly broke the parity-forbidden transition (i.e., dark transition) of double perovskite $Cs_2AgInCl_6$ bulk crystals by alloying Na^+ and doping Bi^{3+} cations, resulting in a dramatic increase in the PLQY up to 86% mainly from the STE emission.[20] A similar observation of STE emission has been reported for double perovskite $Cs_2AgInCl_6$ in the form of NCs, exhibiting stable white STE emissions.[8,26] On the other hand, the investigation of self-trapping mechanisms in emerging vacancy-ordered layered double perovskite nanocrystals, i.e., $Cs_4M(II)M(III)_2X_{12}$, is still at the infancy stage, which urgently requires in-depth understanding for their full potential.

In this work, we conduct lattice engineering on the established layered double perovskite system of $Cs_4CuIn_2Cl_{12}$ (abbreviated as CCuI hereafter) NCs, by replacing Cu^{2+} with other transition metal ions on the $[M(II)Cl_6]^{4-}$ octahedra, including Co^{2+} and Zn^{2+} cations, to synthesize first-ever colloidal $Cs_4CoIn_2Cl_{12}$ (CCoI) and $Cs_4ZnIn_2Cl_{12}$ (CZnI) NCs (see the schematic in **Figure 1a**). Our density functional theory (DFT) calculations demonstrate that STEs are more easily formed in the lattice of CZnI crystal structure while the reference CCuI tends to limit the formation of STEs, due to the difference in their lattice deformation energies. This theoretical prediction aligns well with the observed longest time-resolved PL (TRPL) lifetime for CZnI NCs and the shortest one for CCuI NCs. Benefiting from the formation of more STEs that relax in a radiative way, a broad PL spectrum with a long tail toward 800 nm was recorded with a highest PLQY of 11.4% for CZnI NCs, which is almost two orders of magnitude higher than that (0.12%) of CCuI NCs. Our transient absorption results also confirm the dramatically extended excited state lifetime of 2.2 ns in the case of CZnI NCs when compared to the highly short one (≈44 ps) of CCuI NCs.

2. Results and Discussion

2.1. Colloidal Synthesis of $Cs_4M(II)In_2Cl_{12}$ NCs

Size-controllable colloidal $Cs_4M(II)In_2Cl_{12}$ NCs were synthesized via a modified hot injection method, which has been reported elsewhere.[18,19] The synthetic details are described in the Supporting Information. Upon the swift injection of Cl precursor into the metal precursors (i.e., Cs^+, $M(II)^{2+}$, In^{3+}) mixed with organic ligands (i.e., oleic acid (OA) and oleylamine (OAm)), the target NCs were rapidly formed within a few seconds at 180 °C owing to the fast ionic metathesis reaction process. The XRD patterns of as-synthesized $Cs_4M(II)In_2Cl_{12}$ NCs are compared in Figure 1b. Compared to the simulated powder XRD pattern of CCuI (see the simulation method in Experimental Section in the Supporting Information), all three NCs in this work exhibit a monoclinic phase with a space group of $C2/m$. Several characteristic peaks allocated at ≈24°, 25°, and 34° correspond to $(\bar{3}11)$, (020), and (222) planes, which represent a typical layered double perovskite structure with distorted $[M(II)Cl_6]$ octahedra, as observed for $Cs_4M(II)Sb_2Cl_{12}$ NCs.[16,18] Notably, these characteristic peaks at such as $(\bar{3}11)$ and (020) in the XRD patterns of CCoI and CZnI NCs show a clear upward shift compared to those in the XRD pattern of reference CCuI NCs, hinting that the lattice distortion degree in as-sandwiched $[M(II)Cl_6]$ octahedra may differ among the three samples. It is noted that some characteristic peaks at such as (511) plane of CCoI and CZnI NCs are weaker compared to that of reference CCuI NCs, likely due to the

T. A. Said
Department Spins in Energy Conversion and Quantum Information Science
Helmholtz-Zentrum Berlin für Materialien und Energie GmbH
Albert-Einstein-Str. 16, 12489 Berlin, Germany

J. Liu
MAX IV Laboratory
Fotongatan 2, Lund 224 84, Sweden

H. Ali-Löytty
Surface Science Group
Faculty of Engineering and Natural Sciences
Tampere University
P.O. Box 692, Tampere FI-33014, Finland

K. Lahtonen
Faculty of Engineering and Natural Sciences
Tampere University
P.O. Box 692, Tampere FI-33014, Finland

S. P. Russo
Theoretical Condensed Matter Physics Laboratory
Australian Research Council (ARC) Centre of Excellence for Exciton Science
RMIT University
Melbourne 3000, Australia

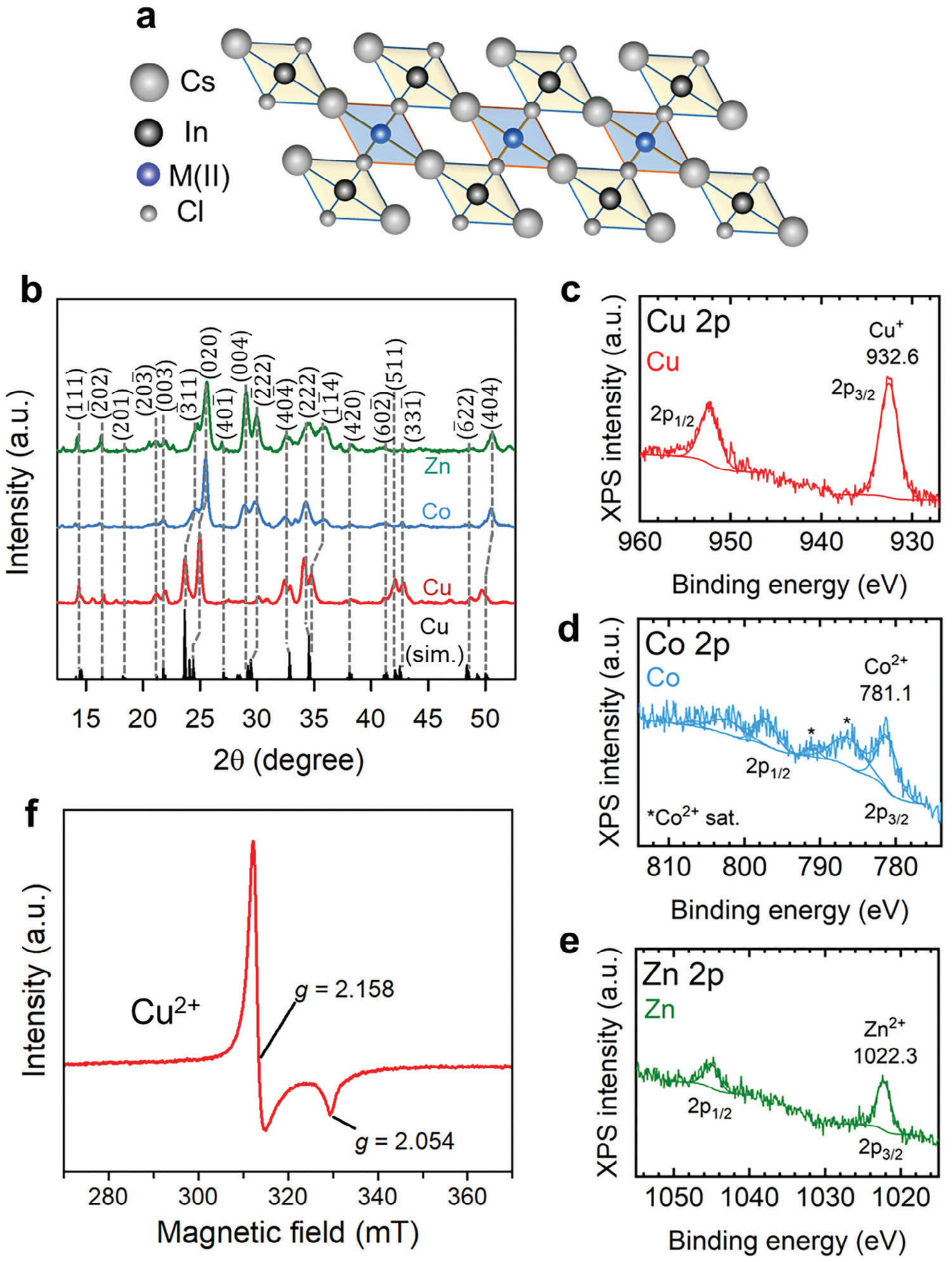

Figure 1. a) Schematic of layered double perovskite $Cs_4M(II)In_2Cl_{12}$ (M(II) = Cu^{2+}, Co^{2+}, Zn^{2+}). b) X-ray diffraction (XRD) patterns of $Cs_4M(II)In_2Cl_{12}$ NCs. The grey dash lines highlight the characteristic peaks, which are compared with the simulated XRD pattern of reference CCuI. X-ray photoelectron core-level spectra (XPS) for $Cs_4M(II)In_2Cl_{12}$ NCs films: c) Cu 2p, d) Co 2p, and e) Zn 2p. f) X-band electron paramagnetic resonance (EPR) spectrum of CCuI NCs at room temperature.

relatively lower crystallinity of CCoI and CZnI NCs at this diffraction angle instead by merging with the adjacent peak at $(33\bar{1})$ in this case. To determine the stoichiometry of as-synthesized NCs, we conducted the energy-dispersive X-ray spectroscopy (EDS) analysis along with the inductively coupled plasma mass spectroscopy (ICP-MS) analysis, which together confirmed the desired stoichiometric ratio of 4:1:2:12 for all three types of layered double perovskite NCs (see Table S1, Supporting Information). The EDS layered images of $Cs_4M(II)In_2Cl_{12}$ NC films for different compositional elements (see Figure S1, Supporting Information) demonstrate the highly homogeneous elemental distribution on the NC film surface. The surface composition of $Cs_4M(II)In_2Cl_{12}$ NCs film samples was analyzed by XPS. Only one chemical state was resolved for the perovskite species Cs (Cs $3d_{5/2}$ at 724.5 eV), Cu (Cu $2p_{3/2}$ at 932.6 eV), Co (Co $2p_{3/2}$ at 781.1 eV), Zn (Zn $2p_{3/2}$ at 1022.3 eV), In (In $3d_{5/2}$ at 445.5 eV), Cl (Cl $2p_{3/2}$ at 198.6), corresponding to Cs^+, Cu^+, Co^{2+}, Zn^{2+}, In^{3+} and Cl^-.[19,22,27] Binding energies of Cs, In, and Cl are close to identical for the three samples (Figure S2, Supporting Information) with different M(II) site cations Cu, Co, and Zn

(Figure 1c–e). Interestingly, out of M(II) site cations, Cu does not appear at the expected divalent state as evidenced by the lack of the characteristic Cu^{2+} shake-up satellite peak at 945–950 eV.[28] The absence of desired Cu^{2+} from the surface is possibly ascribed to the photoreduction of Cu^{2+} to Cu^{+} that Cl evaporation from the surface contributes to the reduction mechanism triggered by X-rays during the measurement.[29,30] Previously, Cai et al. and Zhang et al. reported similar Cu 2p spectrum for Cu at the M(II) site of layered double perovskite $Cs_4CuSb_2Cl_{12}$ and confirmed the presence of Cu^{2+} by their EPR measurements.[18,30] To similarly confirm the oxidation state of Cu, we have conducted the EPR measurement with the X-band EPR spectrum of CCuI NCs at room temperature in Figure 1f. An axial signal with the g values of $g_{\perp} = 2.158$ and $g_{\parallel} = 2.054$ originating from the Cu^{2+} with an unpaired electron spin of $S = 1/2$ ([Ar]$3d^9$ configuration) is clearly observed. The typical Cu hyperfine structure from the $I = 3/2$ nuclear spin is not detected due to the exchange interaction between adjacent Cu^{2+} centers.[31]

The transmission electron microscopy (TEM) images shown in **Figure 2a–c** exhibit that the reference CCuI NCs are formed in a pure cubic-like shape with an average size of 17.3 ± 1.2 nm, which is consistent with previously reported NCs via a similar synthetic route.[19] In addition to the as-formed nanocubes, some amount of rectangle or small rod-like NCs are observed for CCoI and CZnI by showing larger NC formation with average sizes of 22.1 ± 1.4 nm and 24.5 ± 0.8 nm, respectively, compared to the case of CCuI nanocubes. This suggests that the seeds of CCoI and CZnI tend to grow in 1D direction after forming the small nanocubes, likely due to the rearrangement of capping ligands in terms of diverse ionic radius at nuclei position between Co^{2+} (0.68 Å)/Zn^{2+} (0.70 Å) and Cu^{2+} (0.65 Å) ions.[32] The high-resolution TEM (HRTEM) images (Figure 2d–f) confirm the highly crystalline structure in all cases. The lattice *d*-spacings were measured and found to decrease in the order of CCuI (0.375 nm), CCoI (0.371 nm), and CZnI (0.369 nm), and were assigned to the (020) crystal plane. Our fast Fourier transform (FFT) analysis shown in Figure 2d–f further verifies the plane assignment in the HRTEM images, as similarly observed for other type of layered double perovskite NCs.[16] This indicates that the as-synthesized CM(II)I NCs in this work indeed feature the layered perovskite structure with diverse lattice distortion degrees, which is in good agreement with the previous XRD data.

2.2. Optical and Photophysical Properties of $Cs_4M(II)In_2Cl_{12}$ NCs

The absorption spectra of as-synthesized $Cs_4M(II)In_2Cl_{12}$ NC suspensions shown in **Figure 3a** demonstrate that all the exciton peaks of three NC samples fall in the UV range below 325 nm (see the inset in Figure 3a). Note that the multiple absorption bands observed at 600–725 nm in the case of CCoI NCs were assigned to the formation of tetrahedral $[CoCl_4]^{2-}$ ions,[33] which is one type of metal to ligand charge transfer (MLCT) involving weak *d–d* transition. The formation of $[CoCl_4]$ tetrahedra could be considered as a minor side effect during the NC synthesis since the XRD data and EDS analysis have confirmed the desired crystal structure and stoichiometry of $Cs_4CoIn_2Cl_{12}$. Our Tauc analysis (see Figure S3, Supporting Information) verified the direct bandgap nature of all three NCs with an increase in the bandgap from reference CCuI (3.60 eV) to CCoI (3.63 eV) and then to CZnI (3.74 eV) NCs, which are in agreement with the reported direct transition features for other In-based double perovskites.[20,34] Compared to the weak emission of CCuI NCs centered at ≈380 nm, the much stronger and redshifted emissions of both CCoI and CZnI NCs are observed which are centered at ≈416 and ≈430 nm (See Figure 3b), respectively. Notably, the absolute PLQY (0.12%) of reference CCuI NCs has been dramatically enhanced to 4.3% for CCoI NCs and 11.4% for CZnI NCs, which represents nearly two orders of magnitude improvement. In addition, the PL spectra of CCoI and CZnI NCs demonstrate asymmetric and broad PL profiles (as evidenced by the wide full width at half maximum) with long tails toward ≈700 nm and ≈800 nm, respectively, which are recognized as warm white-like emitting lights under the UV light excitation (see the inset photos in Figure 3b). We attribute this significant emission enhancement to the formation of more STE states that relax in a radiative way in the cases of CCoI and CZnI NCs compared to the case of reference CCuI NCs with a limited number of STEs. It is noteworthy that the Stokes shifts of CCoI and CZnI NCs yield just above 100 nm, which are not as large as the reported (>150 nm) for other types of double perovskites that possess STE states,[8,35] likely due to the relatively low self-trapping energy in the soft lattices of this kind of layered double perovskites, which in turn leads to the emission peaks with relatively high energy. To verify the origin of STE emissions, the PL excitation (PLE) spectra were recorded in Figure 3b. All three NCs exhibit almost identically shaped and characteristic PLE spectra, suggesting that the as-observed emissions stem from the relaxation of the same excited state, which in turn confirms that the MLCT of tetrahedral $[CoCl_4]$ ions has not participated in the excitonic transition process in the case of CCoI NCs. Two PLE peaks at ≈300 and ≈325 nm, were assigned to the direct transition approaching the band edge and the STE states such as Jahn–Teller distortion of the $[M(II)Cl_6]$ octahedra in the excited state, respectively.[19] The optical properties of three NCs are summarized in Table S2 (Supporting Information). Furthermore, we measured the TRPL decays by exciting the NC suspensions at 405 nm, as shown in Figure 3c. All PL decays were fitted well with a tri-exponential function with the fitting results in the inset table in Figure 3c. All effective lifetimes of PL decays fall in the microsecond timescale, corresponding to a typical lifetime scale of STE emissions.[36,37] Particularly, the slow component (t_3 = 2.69 µs) of reference PL decay (CCuI) is extended to 3.15 µs (CCoI) and 5.16 µs (CZnI), respectively, hinting that the relaxation of STEs more follows the radiative transition in the cases of CCoI and CZnI NCs.

To gain insights into the $[M(II)Cl_6]$ octahedral coordination, we measured the EXAFS spectra (Figure S4, Supporting Information) of $Cs_4M(II)In_2Cl_{12}$ NC thin films and conducted the Fourier transform analysis, whose fitting results in R-space (R is effective radical distance) are shown in Figure 3d. The kink point in the growing profile (see the inset in Figure 3d) is detected first in the spectrum of CZnI NCs, followed by CCoI and CCuI NCs, successively. This suggests that the effective radical distance of $[M(II)Cl_6]^{4-}$ octahedra arranges in the order of $Cu^{2+} > Co^{2+} > Zn^{2+}$, in good agreement with previous XRD and HRTEM data that confirm the lattice distortion, i.e., Jahn–Teller distortion, when replacing the reference Cu^{2+} with Co^{2+} or Zn^{2+} cations at M(II) site. The diverse $[M(II)Cl_6]$ octahedral

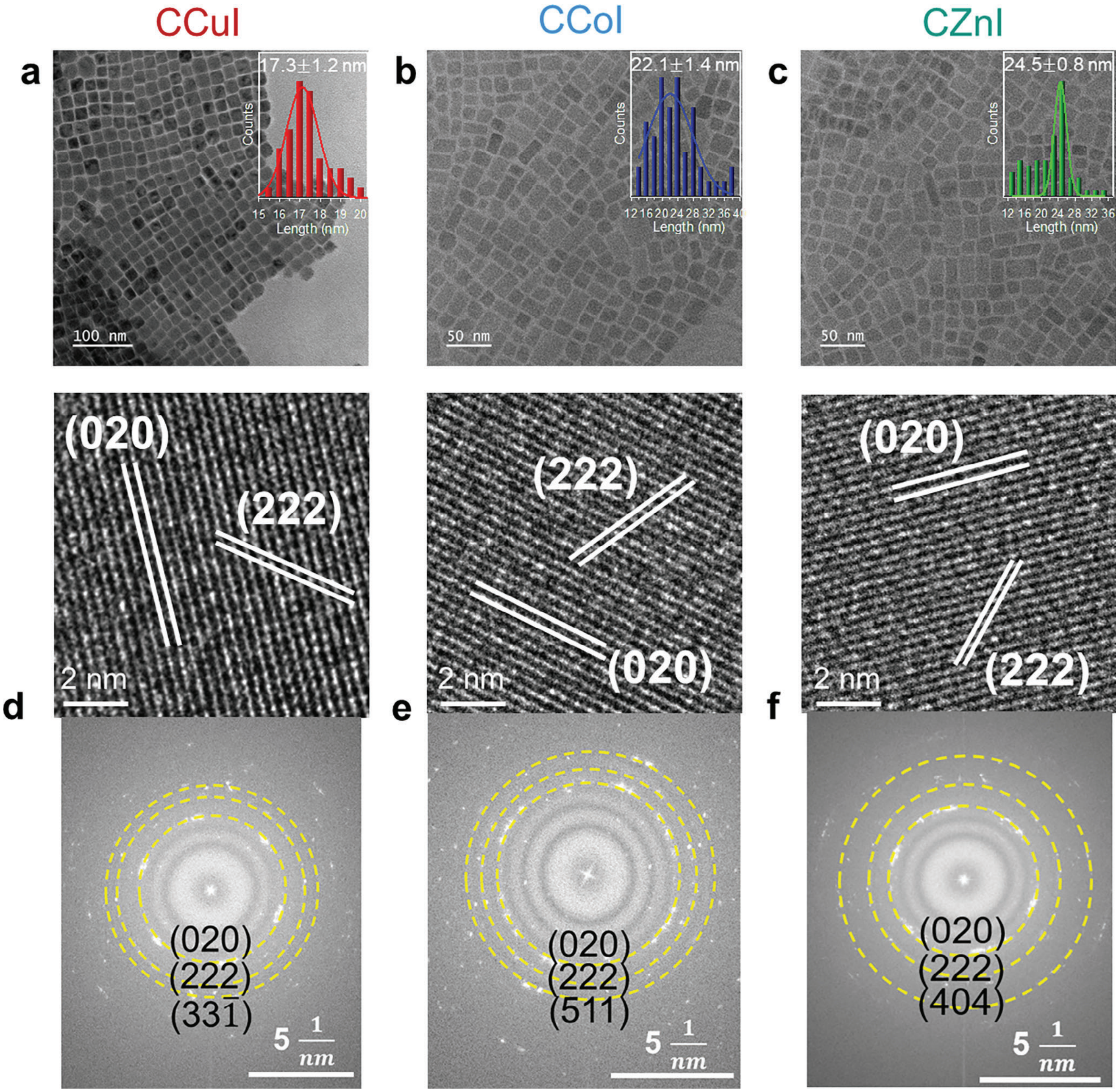

Figure 2. a–c) TEM images and d–f) HRTEM images of $Cs_4M(II)In_2Cl_{12}$ NCs, M(II) = Cu (a,d), Co (b,e) and Zn (c,f). Size distribution histogram of each case is shown in the inset of the corresponding TEM image (a–c). FFT patterns for the HRTEM images are presented under the panels of corresponding HRTEM image (d–f).

coordination could, in turn, influence the interactions between capping ligands (e.g., OA and OAm) and the surface of NCs, which has been identified by measuring the temperature-dependent IR spectra of $Cs_4M(II)In_2Cl_{12}$ NCs as shown in Figure 3e–g. All observed bands in each case become stronger and narrower along with the decrease in the temperature ranging from 300 K to 20 K. Specifically, the featured bands centered at 1572 cm^{-1} were assigned to the $N^+{-}H$ bending bands,[38] which reflect the [NH···Cl] hydrogen-bonding interactions between the OAm ligands and the NCs. Thus, it is reasonable to observe stronger N−H bending bands in the case of reference CCuI NCs since they possess weaker $[CuCl_6]$ octahedral coordination compared to the cases of CCoI and CZnI NCs with stronger lattice distortion. This could also be one cause to drive the NC growth toward 1D or 2D for CCoI and CZnI NCs with weaker OAm confinement effect,[19] as observed in previous TEM images (Figure 2). On the other hand, the characteristic bands between 1420 and 1510 cm^{-1} that correspond to OA ligands (i.e., COO^- stretching),[16] remain almost identical in all three cases, which are less influenced by the $[M(II)Cl_6]$ octahedral coordination.

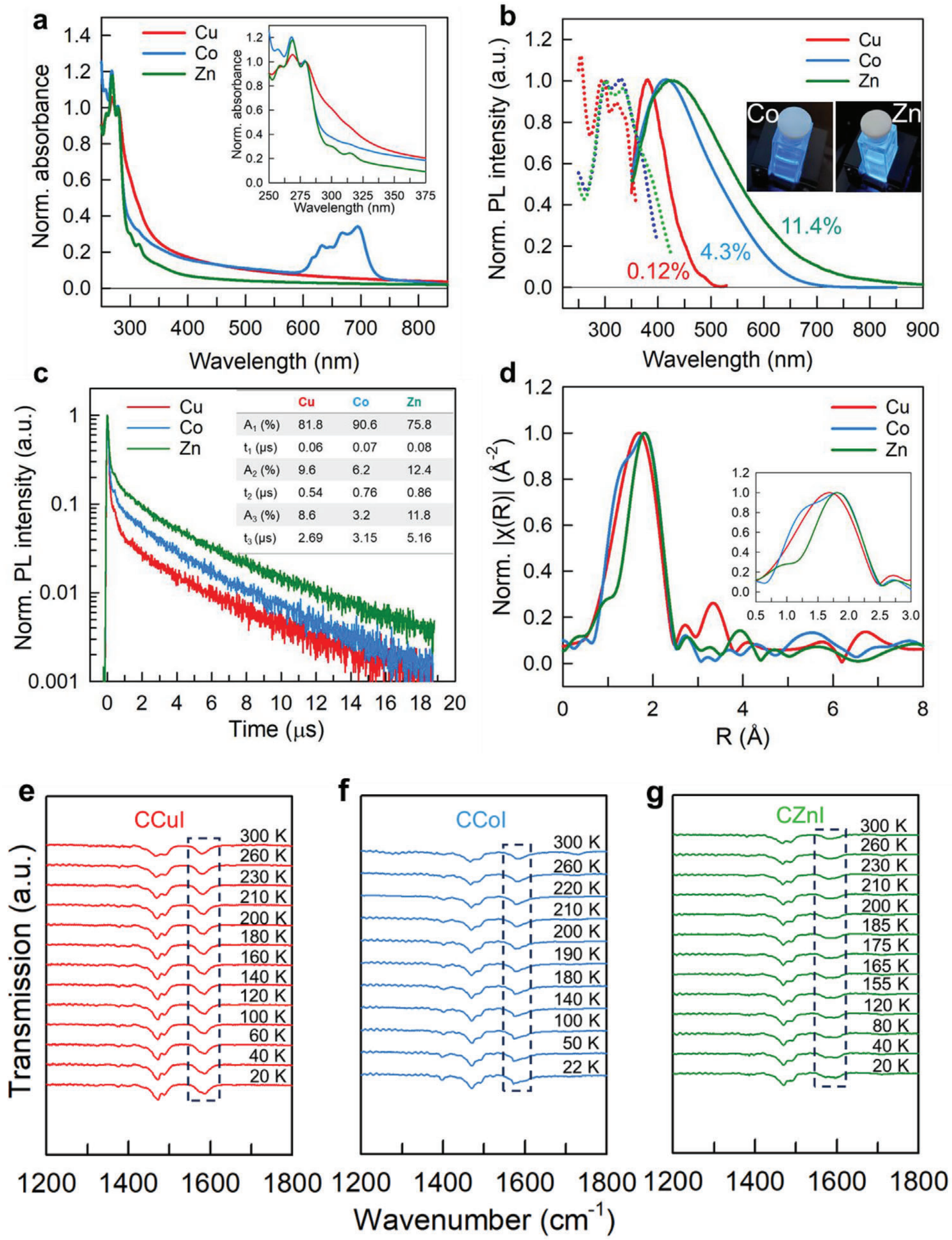

	Cu	Co	Zn
A_1 (%)	81.8	90.6	75.8
t_1 (μs)	0.06	0.07	0.08
A_2 (%)	9.6	6.2	12.4
t_2 (μs)	0.54	0.76	0.86
A_3 (%)	8.6	3.2	11.8
t_3 (μs)	2.69	3.15	5.16

Figure 3. a) Absorption spectra of $Cs_4M(II)In_2Cl_{12}$ (M(II) = Cu, Co, Zn) NCs suspensions with a magnified inset figure in a short wavelength range (250–375 nm). b) Steady-state photoluminescence spectra (excited at 350 nm) and corresponding PLE spectra (in dotted line) of $Cs_4M(II)In_2Cl_{12}$ NCs suspensions. The percentage number highlights the PLQY of each case while the inset figures show the appearance of CCoI and CZnI NCs under the UV light, respectively. c) TRPL decays of $Cs_4M(II)In_2Cl_{12}$ NCs suspensions, excited at 405 nm. The inset table presents the fitting results of TRPL decays with a tri-exponential function. d) Extended X-ray absorption fine structure (EXAFS) spectra of $Cs_4M(II)In_2Cl_{12}$ NCs and fits in R-space. The inset shows the magnified spectra in the early range of R-space. Temperature-dependent infrared (IR) spectra of OA and OAm associated with e) CCuI, f) CCoI, and g) CZnI NCs.

To further investigate the influence of diverse $[M(II)Cl_6]$ octahedra on the photophysical properties of as-synthesized layered double perovskite NCs, the ultrafast transient absorption (TA) measurements were conducted by exciting the NC suspensions at 300 nm and the TA spectra for three NCs at different time delays are presented in **Figure** 4a–c. A strong and broad photoinduced absorption (PIA) at energies across the range of 475–740 nm (upper limitation of our visible detector) is observed for both CCoI and CZnI NCs while a relatively weak and narrow PIA band up to 600 nm was detected within 10 ps after excitation in the case of reference CCuI NCs. This provides direct evidence that more STE states have been formed in either $[CoCl_6]$ or $[ZnCl_6]$ octahedra compared to the $[CuCl_6]$ one, which later contributes to the enhancement of STE emissions via a radiative transition path. In addition, the TA signal size of CZnI NCs is ≈1 mΔO.D., which is almost twice larger than that

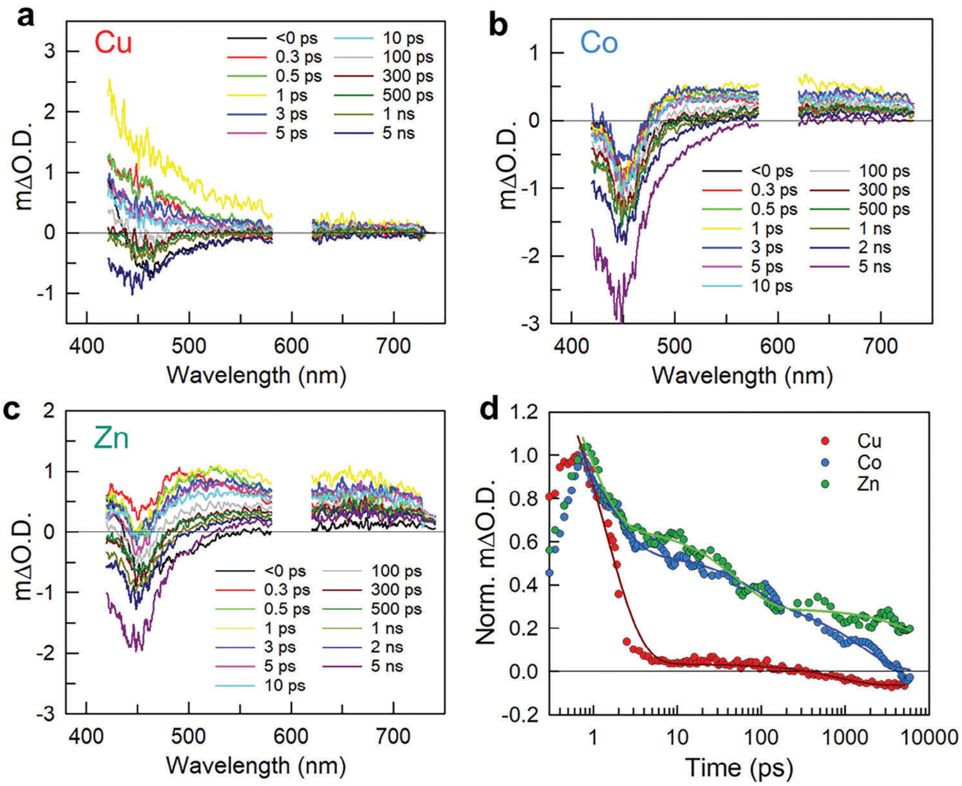

Figure 4. Ultrafast TA spectra of a) CCuI, b) CCoI, and c) CZnI NCs suspensions, excited at 300 nm with an excitation power of 50 µW. The spectral range of 580–620 nm is excluded due to the scattering effect at 600 nm which is doubled excitation wavelength. d) TA decays of CCuI (monitored at 460 nm), CCoI, and CZnI NCs (monitored at 650 nm). Solid lines present the fitting results with a bi-exponential function ($\Delta O.D. = A_1 \exp(-\frac{t}{\tau_1}) + A_2 \exp(-\frac{t}{\tau_2})$) (for CCuI NCs) and a tri-exponential function ($\Delta O.D. = A_1 \exp(-\frac{t}{\tau_1}) + A_2 \exp(-\frac{t}{\tau_2}) + A_3 \exp(-\frac{t}{\tau_3})$) (for CCoI and CZnI NCs), $\Delta O.D.$ is the change of optical density.

(≈0.5 mΔO.D.) of CCoI NCs. This suggests that the lattice structure of CZnI is even more favorable to generate a greater number of STEs under the same excitation condition when compared with the case of CCoI NCs. A negative TA band centered at ≈450 nm is also observed in all cases, which is far away from the excitonic peaks (<350 nm) and thus cannot originate from the ground state bleaching (GSB). We speculate the origin of this negative absorption band to some possible emission (band-to-band) residual from early timescale, which interrupts the broad positive PIA in the whole visible range. The TA decays of three NCs are compared in Figure 3d. The exciton self-trapping process (i.e., TA signal rising stage) completes within 1 ps after excitation, consistent with the reported for other types of double perovskites.[20] The TA profile of reference CCuI NCs follows a bi-exponential decay while the other two decays of CCoI and CZnI NCs can be well-fitted with a tri-exponential function (see the fitting results in Table S3, Supporting Information). The extra third or slow component in the cases of CCoI and CZnI NCs is ascribed to the radiative recombination of STEs,[39] which is almost negligible in the reference case (CCuI NCs). Consequently, the decay lifetime (τ_{AVG} = 43.7 ps) of CCuI NCs has been significantly extended by almost one order and one and a half orders of magnitude for CCoI (τ_{AVG} = 402.7 ps) and CZnI (τ_{AVG} = 2198.6 ps) NCs, respectively. This indeed indicates that the majority of as-formed STE states in the lattice of CZnI NCs relax in a radiative way, possibly benefiting from its suitable lattice deformation energy level which will be theoretically confirmed in the following section.

2.3. Computational Studies of the STEs in $Cs_4M(II)In_2Cl_{12}$ NCs

We further conducted the theoretical analysis to understand the origin of STEs in this type of $Cs_4M(II)In_2Cl_{12}$ NCs. **Figure 5** displays the charge density differential plots from a top-view perspective when observed from the *a*-axis on the *bc*-plane. The charge accumulation in the immediate region around the Zn, Co, and Cu atoms follows the order CZnI > CCoI > CCuI. The initial charge depletion region is immediately followed by an additional charge depletion region. This charge depletion region in turn follows the order of CZnI > CCuI > CCoI. Consequently, the CZnI has roughly equivalent charge accumulation and charge depletion regions stacked on top of each other. In the accumulation and depletion regions, the exciton (a quasiparticle) generated from CZnI, CCuI, or CCoI, exhibits dipole-like behavior and stays for a substantial duration depending on the volumetric charge variance regions. It is worth mentioning that the negative pole (i.e., electron) tends to get trapped in the charge depletion area. While the positive pole (i.e., hole) attempts to remain confined within the charge accumulation region. The strength of such coulombic attraction is determined by the volumetric space

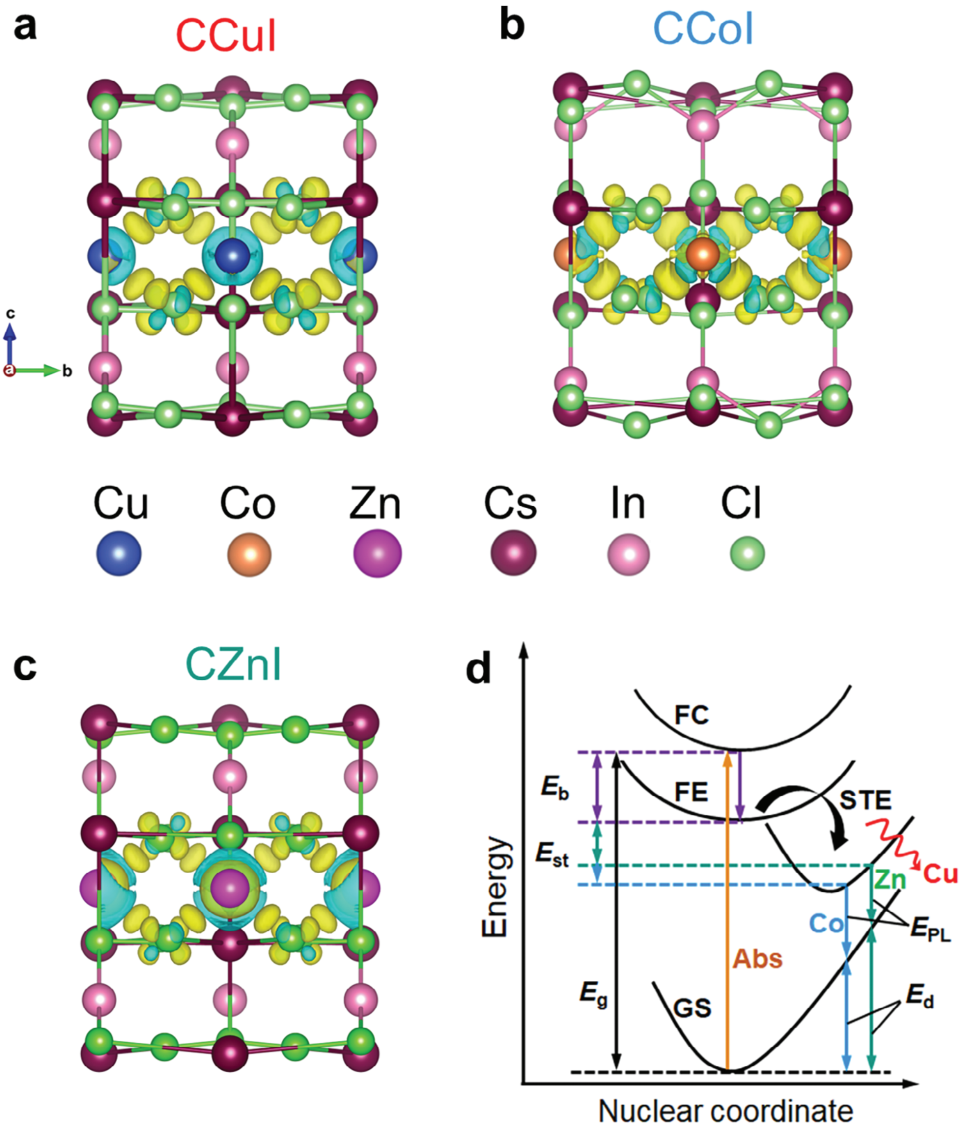

Figure 5. Simulated charge density distribution maps of a) CCuI, b) CCoI, and c) CZnI NCs from the top view. Cyan color represents the charge depletion region, i.e., hole's location, while yellow color indicates the charge accumulation region, i.e., electron's location. All maps are plotted at an iso-surface charge density value of 0.006 electrons Bhor^{-3}. d) Hypothesized configuration coordinate diagram for the STE mechanism of $Cs_4M(II)In_2Cl_{12}$ NCs. FC: free carrier state; FE: free exciton state; E_b: exciton binding energy; E_{st}: self-trapping energy; E_g: bandgap; GS: ground state; Abs: light absorption; E_{PL}: emission energy; E_d: lattice deformation energy.

region in which the charge variation occurs. In this sense, the STE will have a longer lifespan in the following order: CZnI > CCoI > CCuI. The STE lifetime is notably reduced in the surrounding area of the Cu ion because of its pronounced charge depletion and limited accumulation in proximity. In other words, the lifetime of STEs is relatively short when considering a volumetric region, which is the same as that of Zn and Co ions. A thorough understanding of the charge depletion and accumulation regions in the volumetric space is crucial in assessing the mobility of STEs, given their dipole nature. It is clear in all three instances of these models that these regions are arranged diagonally and are linked to the neighboring octahedron composed of indium as the central ion and Cl ions at the corners of the octahedron.

Moreover, the STE generation originating from the [$CoCl_6$] or [$ZnCl_6$] octahedron is confined exclusively within the more distorted octahedron region and subsequently passes through the adjacent Cl atoms in the host octahedron, which is also shared with the neighboring [$InCl_6$] octahedron (see the side-view charge density distribution maps in Figure S5, Supporting Information). Likewise, the anticipated result in all three cases is that the mobility and transit of STEs generated in the [$M(II)Cl_6$] octahedron will align with the adjacent [$InCl_6$] octahedron. This claim is corroborated by our previous photophysical studies, i.e., TRPL lifetimes and excited state lifetimes from TA measurements. However, based on the divergence in volumetric charge density, it can be inferred that the order of STE mobility is potentially CZnI < CCoI < CCuI, ranging from low to high. Applying the same logic, the accumulation and depletion volumes of CCoI occupy a relatively smaller 3D space compared to that of CZnI, but a larger space in the case of CCuI. It is hypothesized that the larger the charge accumulation/depletion region, the longer time the STEs maintain in the region while slowing down their mobility, hence, leading to an extended lifetime. We thus conclude that the STE mobility and lifetime are inversely proportional to each other.

To gain more insight into the formation of lattice-related STEs, we conducted the simulation on the optimized cell lattices of three NC structures, whose lattice parameters are summarized in Table S4 (Supporting Information). It is clearly noted that the lattice distance has been shortened or more distorted both in the *a* and *c* directions (See Figure 5) for CCoI and CZnI structures compared to the reference structure (CCuI), which indicates that the inserted [$CoCl_6$] or [$ZnCl_6$] octahedra can indeed drag more effectively the two adjacent [$InCl_6$] octahedra layers, leading to more distorted lattice structures. In addition, the simulated system energies in the ground state of CCoI (−135.965 eV) and CZnI (−129.071 eV) are obviously lower than that (−122.394 eV) of CCuI, making good agreement with our previous speculation about the role of lattice deformation energy (E_d) in changing their excited states at STE level. We thus propose a dynamic diagram to demonstrate the overall STE mechanism of $Cs_4M(II)In_2Cl_{12}$ NCs in Figure 5d. Upon the generation of free carriers after light harvesting, photogenerated electrons, and holes could be swiftly self-trapped if the electron-phonon interactions are strong enough to induce elastic distortions in the lattice surrounding those free carriers.[37] In the following self-trapping process, the energy loss in this excited state is defined as self-trapping energy E_{st}. In the meanwhile, the ground state energy will increase due to the lattice deformation, as so-called lattice deformation energy E_d. Accordingly, the PL energy can be expressed by $E_{PL} = E_g - E_b - E_{st} - E_d$, where E_g is bandgap and E_b is exciton binding energy at room temperature. In our reference case (CCuI NCs), most self-trapped excitons recombine in a non-radiative way, e.g., phonons, due to the large E_d that leads to the crossing of the excited and ground state curves in the configuration coordinate diagram. In contrast, the lattice deformation energy is just at a suitable level (not too big or too small) in both cases of CCoI and CZnI NCs, resulting in the radiative recombination of most of the STEs that eventually demonstrate much-enhanced PLQYs. It is noteworthy that the E_d of CZnI NCs could be relatively larger than that of CCoI NCs by assuming both possess similar E_b at room temperature, possibly leading to a lower E_{PL} that corresponds to a broader and redshifted STE emission toward white emitting light in the case of CZnI NCs.

3. Conclusion

In summary, we first-ever report the colloidal synthesis of lead-free and wide-band-gap layered double perovskites, $Cs_4CoIn_2Cl_{12}$ and $Cs_4ZnIn_2Cl_{12}$, by tuning the M(II) site with different transition metal ions. Compared to the reference almost non-emissive CCuI NCs, CCoI and CZnI NCs have dramatically improved the PLQYs to 4.3% and 11.4% in the emission light ranges of up to ≈700 and ≈800 nm, respectively. Our DFT calculation results reveal that the photo-generated excitons can be more easily self-trapped in the lattices of [$CoCl_6$] and [$ZnCl_6$] octahedra layers rather than in those of [$CuCl_6$] octahedra, mainly due to the lower lattice deformation energies in the former two cases. The as-formed STEs in CCoI and CZnI NCs are found to recombine more in a radiative way, as evidenced by the extended excited state lifetimes of up to 2.2 ns for CZnI NCs when compared to the extremely short lifetime of 43 ps for CCuI NCs. Our comprehensive theoretical and experimental studies clearly emphasize the importance of lattice engineering in boosting the STE emissions of layered double perovskites at room temperature. The photoluminescent properties of these CM(II)I NCs could be enhanced by further NC size control or impurity cation doping. This work paves the way for new lead-free halide perovskites for eco-friendly warm white light-emitting applications.

Supporting Information

Supporting Information is available from the Wiley Online Library or from the author.

Acknowledgements

M.L. acknowledges the Royal Physiographic Society of Lund and the Finnish Cultural Foundation (No. 00220107) for the financial support. This work was partially supported by the Wallenberg Initiative Materials Science for Sustainability (WISE) funded by the Knut and Alice Wallenberg Foundation. S.K.M. acknowledges JSPS for the computational analysis work was conducted with the support from JSPS KAKENHI Grant Number JP22F32733, through the host institution Centre of Computational Sciences, University of Tsukuba, Japan. S.K.M. also acknowledges the FUJITSU Supercomputer PRIMEHPC FX1000 and FUJITSU Server PRIMERGY GX2570 (Wisteria/BDEC-01) facilities at the Information Technology Center, The University of Tokyo. S.K.M. and S.P.R. thank the partial support provided by the Australian Research Council (ARC) through the Centre of Excellence scheme (Project No. CE170100026), generously funded by the Australian government. J.L. acknowledges MAXIV: SSF ITM-170276 for financial support. B.A.-A. thanks Vilho, Yrjö and Kalle Väisälä Fund of the Finnish Academy of Science and Letters for financial support. P.V. acknowledges the financial support of Jane and Aatos Erkko Foundation within the SOL-TECH project. This work was part of the Academy of Finland Flagship Programme, Photonics Research, and Innovation (PREIN), Decision No. 320165 and No. 346511. This work made use of Tampere Microscopy Center facilities at Tampere University.

Conflict of Interest

The authors declare no conflict of interest.

Data Availability Statement

The data that support the findings of this study are available from the corresponding author upon reasonable request.

Keywords

lattice engineering, layered double perovskite nanocrystals, photoluminescence quantum yield, self-trapped exciton, transition metal ions

Received: February 8, 2024
Revised: May 20, 2024
Published online:

[1] A. Karmakar, M. S. Dodd, S. Agnihotri, E. Ravera, V. K. Michaelis, *Chem. Mater.* **2018**, *30*, 8280.
[2] N. P. Holzapfel, J. D. Majher, T. A. Strom, C. E. Moore, P. M. Woodward, *Chem. Mater.* **2020**, *32*, 3510.
[3] J. D. Majher, M. B. Gray, T. A. Strom, P. M. Woodward, *Chem. Mater.* **2019**, *31*, 1738.
[4] K. Du, W. Meng, X. Wang, Y. Yan, D. B. Mitzi, *Angew. Chem., Int. Ed.* **2017**, *56*, 8158.
[5] Y. Bekenstein, J. C. Dahl, J. Huang, W. T. Osowiecki, J. K. Swabeck, E. M. Chan, P. Yang, A. P. Alivisatos, *Nano Lett.* **2018**, *18*, 3502.
[6] M. Liu, H. Zhang, D. Gedamu, P. Fourmont, H. Rekola, A. Hiltunen, S. G. Cloutier, R. Nechache, A. Priimagi, P. Vivo, *Small* **2019**, *15*, 1900801.
[7] S. E. Creutz, E. N. Crites, M. C. De Siena, D. R. Gamelin, *Nano Lett.* **2018**, *18*, 1118.
[8] F. Locardi, M. Cirignano, D. Baranov, Z. Dang, M. Prato, F. Drago, M. Ferretti, V. Pinchetti, M. Fanciulli, S. Brovelli, L. De Trizio, L. Manna, *J. Am. Chem. Soc.* **2018**, *140*, 12989.
[9] S. E. Creutz, H. Liu, M. E. Kaiser, X. Li, D. R. Gamelin, *Chem. Mater.* **2019**, *31*, 4685.
[10] L. Zhang, K. Wang, B. Zou, *ChemSusChem* **2019**, *12*, 1612.
[11] B. Yang, J. Chen, S. Yang, F. Hong, L. Sun, P. Han, T. Pullerits, W. Deng, K. Han, *Angew. Chem., Int. Ed.* **2018**, *57*, 5359.
[12] J. Shamsi, A. S. Urban, M. Imran, L. De Trizio, L. Manna, *Chem. Rev.* **2019**, *119*, 3296.
[13] I. López-Fernández, D. Valli, C. Y. Wang, S. Samanta, T. Okamoto, Y. T. Huang, K. Sun, Y. Liu, V. S. Chirvony, A. Patra, J. Zito, L. De Trizio, D. Gaur, H. T. Sun, Z. Xia, X. Li, H. Zeng, I. Mora-Seró, N. Pradhan, J. P. Martínez-Pastor, P. Müller-Buschbaum, V. Biju, T. Debnath, M. Saliba, E. Debroye, R. L. Z. Hoye, I. Infante, L. Manna, L. Polavarapu, *Adv. Funct. Mater.* **2024**, *34*, 2307896.
[14] A. Dey, J. Ye, A. De, E. Debroye, S. K. Ha, E. Bladt, A. S. Kshirsagar, Z. Wang, J. Yin, Y. Wang, L. N. Quan, F. Yan, M. Gao, X. Li, J. Shamsi, T. Debnath, M. Cao, M. A. Scheel, S. Kumar, J. A. Steele, M. Gerhard, L. Chouhan, K. Xu, X. G. Wu, Y. Li, Y. Zhang, A. Dutta, C. Han, I. Vincon, A. L. Rogach, *ACS Nano* **2021**, *15*, 10775.
[15] B. Vargas, E. Ramos, E. Pérez-Gutiérrez, J. C. Alonso, D. Solis-Ibarra, *J. Am. Chem. Soc.* **2017**, *139*, 9116.
[16] H. Mai, X. Li, J. Lu, X. Wen, T. C. Le, S. P. Russo, D. Chen, R. A. Caruso, *J. Am. Chem. Soc.* **2023**, *145*, 17337.
[17] X. D. Wang, N. H. Miao, J. F. Liao, W. Q. Li, Y. Xie, J. Chen, Z. M. Sun, H. Y. Chen, D. Bin Kuang, *Nanoscale* **2019**, *11*, 5180.
[18] T. Cai, W. Shi, S. Hwang, K. Kobbekaduwa, Y. Nagaoka, H. Yang, K. Hills-Kimball, H. Zhu, J. Wang, Z. Wang, Y. Liu, D. Su, J. Gao, O. Chen, *J. Am. Chem. Soc.* **2020**, *142*, 11927.
[19] M. Liu, S. K. Matta, H. Ali-Löytty, A. Matuhina, G. K. Grandhi, K. Lahtonen, S. P. Russo, P. Vivo, *Nano Lett.* **2022**, *22*, 311.
[20] J. Luo, X. Wang, S. Li, J. Liu, Y. Guo, G. Niu, L. Yao, Y. Fu, L. Gao, Q. Dong, C. Zhao, M. Leng, F. Ma, W. Liang, L. Wang, S. Jin, J. Han, L. Zhang, J. Etheridge, J. Wang, Y. Yan, E. H. Sargent, J. Tang, *Nature* **2018**, *563*, 541.
[21] B. M. Benin, D. N. Dirin, V. Morad, M. Wörle, S. Yakunin, G. Rainò, O. Nazarenko, M. Fischer, I. Infante, M. V. Kovalenko, *Angew. Chem., Int. Ed.* **2018**, *57*, 11329.
[22] R. Scholz, A. Y. Kobitski, D. R. T. Zahn, M. Schreiber, *Phys. Rev. B* **2005**, *72*, 245208.
[23] D. Menzel, *Appl. Phys. A* **1990**, *51*, 163.
[24] W. B. Fowler, M. J. Marrone, M. N. Kabler, *Phys. Rev. B* **1973**, *8*, 5909.
[25] R. T. Williams, K. S. Song, W. L. Faust, C. H. Leung, *Phys. Rev. B* **1986**, *33*, 7232.
[26] Y. Liu, Y. Jing, J. Zhao, Q. Liu, Z. Xia, *Chem. Mater.* **2019**, *31*, 9522.
[27] A. V. Naumkin, A. Kraut-Vass, C. J. Powell, *NIST XPS Database* **2008**, 20.
[28] M. C. Biesinger, *Surf. Interface Anal.* **2017**, *49*, 1325.
[29] D. C. Frost, A. Ishitani, C. A. McDowell, *Mol. Phys.* **1972**, *24*, 861.
[30] K. Zhang, Y. Zhang, D. Zhou, Y. Yang, Z. Yang, Z. Song, J. Zhang, Q. Wang, J. Qiu, *J. Alloys Compd.* **2024**, *976*, 173283.
[31] N. Singhal, R. Chakraborty, P. Ghosh, A. Nag, *Chem. – An Asian J.* **2018**, *13*, 2085.
[32] Atomistic Simulation Group in the Materials Department of Imperial College, Database of Ionic Radii, http://abulafia.mt.ic.ac.uk/shannon/ptable.php (accessed: May 2024).
[33] M. Uchikoshi, *J. Solution Chem.* **2018**, *47*, 2021.
[34] G. Volonakis, A. A. Haghighirad, R. L. Milot, W. H. Sio, M. R. Filip, B. Wenger, M. B. Johnston, L. M. Herz, H. J. Snaith, F. Giustino, *J. Phys. Chem. Lett.* **2017**, *8*, 772.
[35] B. Yang, F. Hong, J. Chen, Y. Tang, L. ang, Y. Sang, X. Xia, J. Guo, H. He, S. Yang, W. Deng, K. Han, *Angew. Chem.* **2019**, *131*, 2300.
[36] A. Matuhina, G. K. Grandhi, F. Pan, M. Liu, H. Ali-Löytty, H. M. Ayedh, A. Tukiainen, J. H. Smått, V. Vähänissi, H. Savin, J. Li, P. Rinke, P. Vivo, *ACS Appl. Nano Mater.* **2023**, *6*, 953.
[37] S. Li, J. Luo, J. Liu, J. Tang, *J. Phys. Chem. Lett.* **2019**, *10*, 1999.
[38] A. Pan, B. He, X. Fan, Z. Liu, J. J. Urban, A. P. Alivisatos, L. He, Y. Liu, *ACS Nano* **2016**, *10*, 7943.
[39] B. Yang, K. Han, *J. Phys. Chem. Lett.* **2021**, *12*, 8256.